Available online at www.sciencedirect.com
ScienceDirect
Biomaterials 28 (2007) 2438–2445
Biomaterials
www.elsevier.com/locate/biomaterials

Non-invasive evaluation of alginate/poly-L-lysine/alginate microcapsules by magnetic resonance microscopy

Ioannis Constantinidis[a,b,*,1], Samuel C. Grant[b,c,d,1,2], Susanne Celper[e], Isabel Gauffin-Holmberg[e], Kristina Agering[e], Jose A. Oca-Cossio[a], Jonathan D. Bui[d], Jeremy Flint[c,d], Christine Hamaty[a], Nicholas E. Simpson[a], Stephen J. Blackband[b,c,d]

[a]*Division of Endocrinology, Department of Medicine, University of Florida, PO Box 100226, Gainesville, FL 32610-0226, USA*
[b]*National High Magnetic Field Laboratory, Tallahassee, FL 32310, USA*
[c]*Department of Neuroscience, University of Florida, Gainesville, FL 32610, USA*
[d]*McKnight Brain Institute, University of Florida, Gainesville, FL 32610, USA*
[e]*Royal Institute of Technology and the Royal Karolinska Medical and Surgical Institute, Stockholm, Sweden*

Received 21 July 2006; accepted 1 January 2007
Available online 8 January 2007

Abstract

In this report, we present data to demonstrate the utility of ^{1}H MR microscopy to non-invasively examine alginate/poly-L-lysine/alginate (APA) microcapsules. Specifically, high-resolution images were used to visualize and quantify the poly-L-lysine (PLL) layer, and monitor temporal changes in the alginate gel microstructure during a month long *in vitro* culture. The thickness of the alginate/PLL layer was quantified to be $40.6 \pm 6.2\,\mu m$ regardless of the alginate composition used to generate the beads or the time of alginate/PLL interaction (2, 6, or 20 min). However, there was a notable difference in the contrast of the PLL layer that depended upon the guluronic content of the alginate and the alginate/PLL interaction time. The T_2 relaxation time and the apparent diffusion coefficient (ADC) of the alginate matrix were measured periodically throughout the month long culture period. Alginate beads generated with a high guluronic content alginate demonstrated a temporal decrease in T_2 over the duration of the experiment, while ADC was unaffected. This decrease in T_2 is attributed to a reorganization of the alginate microstructure due to periodic media exchanges that mimicked a regular feeding regiment for cultured cells. In beads coated with a PLL layer, this temporal decrease in T_2 was less pronounced suggesting that the PLL layer helped maintain the integrity of the initial alginate microstructure. Conversely, alginate beads generated with a high mannuronic content alginate (with or without a PLL layer) did not display temporal changes in either T_2 or ADC. This observation suggests that the microstructure of high mannuronic content alginate beads is less susceptible to culture conditions.

Keywords: MR imaging; Alginate encapsulation; Poly-L-lysine

1. Introduction

Evaluation of tissue engineered constructs by non-invasive imaging techniques can focus on the cellular component of the constructs—providing information critical to their function—or the biomaterials utilized in making the constructs—providing information critical to their structural integrity. Both tasks are equally important and synergistic to understanding the structure/function relationship of a construct under examination. Nuclear Magnetic Resonance (NMR) is a versatile, non-invasive

*Corresponding author. Division of Endocrinology, Department of Medicine, University of Florida, PO Box 100226, Gainesville, FL, 32610-0226, USA.
E-mail address: consti@medicine.ufl.edu (I. Constantinidis).
[1]Both authors have contributed equally to this study.
[2]Current address: Department of Chemical & Biomedical Engineering, The Florida State University & National High Magnetic Field Laboratory, Tallahassee, FL 32310, USA.

0142-9612/$ - see front matter © 2007 Elsevier Ltd. All rights reserved.
doi:10.1016/j.biomaterials.2007.01.012

modality with a range of active nuclei and contrast mechanisms that has the ability to provide both metabolic and structural information. Although the use of NMR in medical and biological research is widespread, its application to tissue engineering has been limited [1–3].

In the development of a bioartificial pancreas, most studies employing NMR techniques have focused on ^{31}P and ^{1}H NMR spectroscopy to investigate the correlation between cellular metabolism and insulin secretion under various environmental conditions [4–8]. One of the conclusions derived by ^{1}H NMR was that the resonance at 3.20 ppm, attributed to the trimethylamine protons of choline and its phosphorylated mono- and diesters, was sensitive to the overall metabolic activity of encapsulated cells maintained within a perfusion bioreactor [8]. This resonance was subsequently utilized to quantify viable cell numbers within a disk-shaped pancreatic construct both *in vitro* and *in vivo* [9,10]. Although these studies provide invaluable information on the cellular function of the construct, they do not offer insight into potential structural changes of the biomaterials utilized.

The ability to monitor the structural integrity of a tissue engineered construct either *in vitro* or *in vivo* is critical in evaluating or predicting its structural demise. This assessment is particularly important for alginate-based constructs that have been known to deteriorate with time. Alginate is a naturally occurring biopolymer that has been used extensively as a vehicle to encapsulate a variety of biological materials including enzymes and cells of both microbial and mammalian origin. However, its long-term structural integrity is questioned given the soft gelatinous nature of the material. In tissue engineering, and particularly in the development of a bioartificial pancreas, alginates have been used to encapsulate islets [11–14] and transformed β-cells [4,15–17] with considerable success. A layer of a polycation, such as poly-L-lysine (PLL), followed by an additional layer of alginate is commonly used to coat the central alginate matrix, providing mechanical stability to the matrix [18] and at least partial immunoprotection [19].

Magnetic resonance (MR) imaging at microscopic resolutions ($<100\,\mu m$), commonly referred to as MR microscopy, has been used to monitor alginate beads [20–25] immediately following encapsulation or shortly thereafter, but has not been used to track alginate beads during a long-term culture. Because changes in the T_2 relaxation time have been shown to correlate with changes in material porosity [26], we postulated that MR microscopy could be used to examine alginate/poly-L-lysine/alginate (APA) microcapsules integrity over time. In this report, ^{1}H MR microscopy was employed to (i) visualize and quantify the thickness of the PLL layer by taking advantage of the contrast generated by the interaction between alginate and PLL and (ii) monitor temporal changes in alginate gel microstructure by quantifying the MR properties of the alginate matrix.

2. Methods

2.1. Alginate microcapsules

Two types of alginate were used in this study (FMC BioPolymer, Drammen, Norway): (i) a high guluronic content alginate (MVG) composed of 73% guluronic acid (60% consecutive guluronic residues) and 27% mannuronic acid (manufacturer's data); and (ii) a high mannuronic content alginate (MVM) composed of 38% guluronic acid (20% consecutive guluronic residues) and 62% mannuronic acid (manufacturer's data). All alginate solutions were prepared by dissolving powder alginate in physiological saline (0.85% NaCl) at a concentration of 2% (w/v). The presence of non-crosslinking Na^+ ions generates a more homogeneous gel bead [27]. Alginate beads were generated with the aid of an electrostatic bead generator (Nisco, Basel, Switzerland) by crosslinking alginate with 100 mM $CaCl_2$. APA beads were produced based on the protocol developed by Lim and Sun [13] and modified to suit our requirements [16]. Briefly, alginate beads were washed with solutions of $CaCl_2$, CHES, 0.05% PLL and 0.2% alginate (of the same type as that used for the core material) to create the final APA beads at a diameter of $750\pm50\,\mu m$. The APA beads in this study were not treated with citrate to liquefy the central alginate core.

To assess differences in the alginate/PLL interaction, two PLL polymers were tested; one of low molecular weight (19,200 g/mol) and one of higher molecular weight (240,000 g/mol) (Sigma, St. Louis, MO). Furthermore, alginate beads were exposed to a 0.05% PLL solution for either 2, 6 or 20 min. Table 1 shows the various combinations of alginate composition, PLL molecular weight and interaction times examined. From the time the beads were generated to the end of the experiment, they were maintained in Dulbecco's Minimum Essential Medium (DMEM; Sigma, St. Louis, MO).

Temporal effects due to a 30 days long *in vitro* culture on alginate gel microstructure were assessed on both PLL coated and uncoated alginate beads composed of either MVG or MVM alginate. For these longitudinal experiments, alginate beads were coated with the lower molecular weight PLL using an exposure time of 6 min. The beads were maintained in a fashion similar to the culture of encapsulated cells; the DMEM medium was changed with fresh medium three times weekly. Because all experiments presented in this study were performed with cell-free alginate beads, temporal changes reflect the effect of frequent media switches, characteristic of *in vitro* cell culture, on the microstructure of the alginate gel without the confounding effects of cell growth and/or metabolic activity, which may contribute to these changes as well.

2.2. MR microscopy

All MR images were acquired using a vertical 17.6-T 89-mm bore cryopumped magnet equipped with a Bruker Avance console and Micro2.5 gradients (maximum strength of 1 T/m). Three to six beads immersed in DMEM were loaded into a glass capillary (inner diameter,

Table 1
Combinations of alginate composition, PLL molecular weight and time of interaction between alginate and PLL examined

Alginate type	MVM						MVG					
Molecular weight of PLL (Da)	Low (19,200)			High (240,000)			Low (19,200)			High (240,000)		
Exposure time (min)	2	6	20	2	6	20	2	6	20	2	6	20

1 mm) that was placed within a homebuilt solenoidal microcoil (6 mm length, 1.7 mm in diameter). Coupled with the high magnetic field, these small RF solenoids greatly improve the sensitivity of the NMR experiment and are susceptibility-matched to reduce magnetic field perturbations [28].

The images presented here were acquired using a gradient recall echo (GRE) sequence with averaging (NEX) = 4, echo time (TE) = 7.5, 15 and 25 ms, recovery time (TR) = 150 ms, matrix (MTX) of $512 \times 128 \times 128$, field of view (FOV) of $6.4 \times 1.6 \times 1.6\,mm^3$. Thus, an isotropic spatial resolution of 12.5 μm for each image was acquired in approximately 2.75 h. To assess the contribution of T_2* in the detection of the PLL layer, GRE images of high mannuronic content APA beads were collected at variable TEs (4–40 ms) or variable bandwidths (15,000–100,000 Hz). These images were obtained by holding one of the two acquisition parameters (i.e. TE and bandwidth) constant while varying the other. For these T_2* assessments, APA beads were composed of the lower molecular weight PLL and the time that the PLL solution was allowed to interact with the alginate beads was 6 min.

MR images were also acquired using a conventional spin-echo (SE) imaging sequence that employed a bipolar read-refocusing gradient pair located after the second radio frequency pulse to minimize the effect of unintended water diffusion resulting from the read gradient [29]. To quantify T_2, separate images were acquired at echo times ranging from 15 to 120 ms. These T_2-weighted images were acquired in 25.5 min/image with NEX = 4, TR = 1.5 s, MTX = 512×256, FOV of $2.4 \times 1.2\,cm^2$ and slice thickness of 60 μm. Diffusion weighted images were acquired at five diffusion weightings using the same spin echo sequence and by incrementing the diffusion gradient strength (b values = 195, 507, 748, 977 and 1200 s/mm^2). All other imaging parameters remained constant between images. The nominal resolution of both T_2- and diffusion-weighted images was $47 \times 47 \times 60\,\mu m^3$. Quantification of T_2 relaxation and the apparent diffusion coefficient (ADC) was performed based on a region of interest (ROI) analysis. Circular ROIs encompassing the entire bead and the center of the bead were generated and the average signal intensity over the entire ROI was measured. Based on these measurements, the T_2 relaxation time and the ADC were calculated by fitting signal intensity as a function of TE or b value respectively using a non-linear Levenberg-Marquardt regression analysis for a single decaying exponential function. The total acquisition time for quantitative imaging experiments on a single bead preparation was 6.5 h.

2.3. Quantification of the PLL layer

The amount of PLL deposited on the alginate matrix was quantified by measuring the concentration of the PLL solution before and after exposure to the alginate beads. Briefly, samples of the PLL solution were collected before and after exposure with alginate beads, lyophilized and dissolved in 100 μl of saline. Ten microliters of the resuspended solution were placed in different wells within a 96-well-plate, and 100 μl of a fluorescamine (Sigma, St. Louis, MO) solution (3 mg of fluorescamine per ml of DMSO) were added to each well. The microwell plate was placed in a Synergy HT plate reader (Bio-Tek, Winooski, VT) and allowed to incubate at 37 °C for 20 min. Fluorescence was measured using an excitation filter centered at 360 nm with a bandwidth of 40 nm and an emission filter centered at 460 nm with a bandwidth of 10 nm. The values measured from our samples were compared against a calibration curve of known PLL concentrations. The amount of PLL deposited per ml of beads was calculated by subtracting the measurements before and after exposure. Thus, when small quantities of PLL are deposited on the beads, the error in this measurement is large. Each measurement was performed twice and a t-test analysis was used to determine the statistical significance of the results.

3. Results

3.1. Visualization and quantification of the PLL layer

Fig. 1 illustrates SE images (TE = 25 and 65 ms) of four MVM beads. The bottom two beads are coated with a PLL layer (lower molecular weight PLL with 6 min exposure time) while the top two are not coated with PLL. The non-coated beads show a faint ring around the bead attributed to a small susceptibility (T_2*) effect induced by the gel/media interface. The PLL coated beads show a dark circle at the periphery of the alginate matrix that clearly demarcates the beads from the surrounding medium. Compared to the signal intensity of the (a) inner bead and (b) external media, the PLL layer in Fig. 1 shows a contrast enhancement of (a) $27 \pm 5\%$ and (b) $39 \pm 2\%$, respectively, for a TE = 25 ms and an enhancement of (a) $54 \pm 0.8\%$ and (b) $70 \pm 0.07\%$ for a TE = 65 ms. For reference, the periphery of the uncoated beads in Fig. 1 displays a contrast enhancement of only 3.5 ± 0.8 to $4.8 \pm 8.8\%$ compared to the interior of the bead. These averages and standard deviations were determined based on $n = 7$ measurements. Additionally, the thickness of the observed layer did not increase by increasing either TE or decreasing bandwidth and was the same for both SE and GRE images (data not shown). These observations suggest that the contrast generated by the PLL layer is largely due to intrinsic T_2 relaxation with a small contribution by local field inhomogeneities. Conversely, the contrast generated by the small air bubble located on the top PLL coated bead, is dominated by T_2* as demonstrated by the increase in its size with increasing TE. However, it is possible that T_2* contribution may be underestimated given the limited number of pixels across the PLL layer.

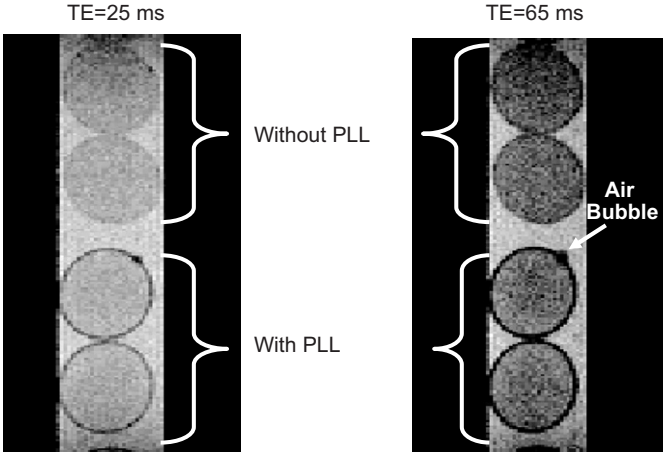

Fig. 1. Spin echo MR microimages of MVM alginate beads with and without PLL coating (6 min exposure to low molecular weight PLL) at two different echo times. Note that the dark circle around the alginate beads coated with PLL does not significantly change in size with longer TE—unlike the air bubble (white arrow).

Fig. 2 shows GRE images illustrating differences in the alginate/PLL contrast as a function of the alginate composition and the exposure time between alginate beads and the PLL solution. Specifically, for alginate beads coated with the lower molecular weight PLL, the contrast due to the PLL layer increased as the interaction time between alginate and PLL increased from 2 to 6 to 20 min. This effect was observed for both alginate compositions

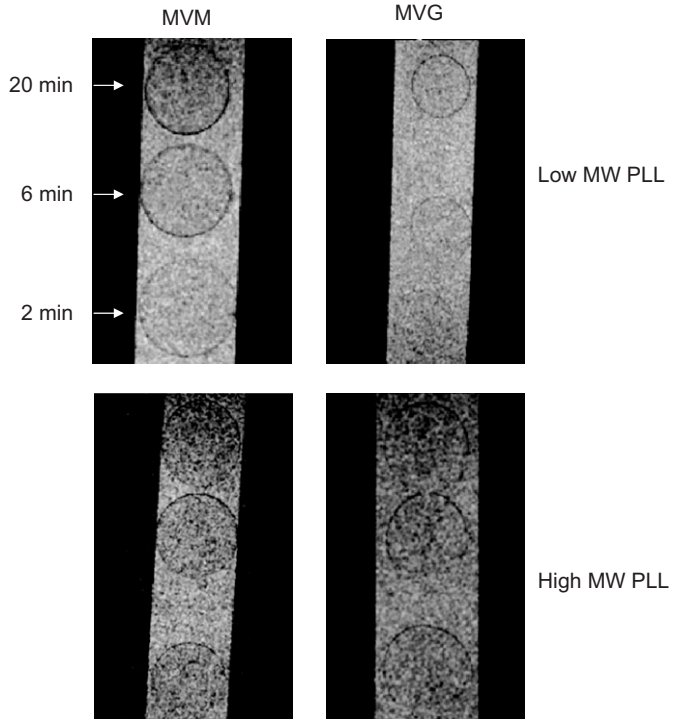

Fig. 2. GRE MR microimages of MVM APA beads showing the intensity of the PLL layer as a function of alginate composition and interaction time. The isotropic resolution of these images is 12.5 μm.

examined, but it was more pronounced for beads generated with MVM alginate. However, when the high molecular weight PLL polymer was used, there were no distinguishable differences in contrast as a function of either interaction times or alginate composition. To quantify these alterations in contrast, the signal-to-noise ratio (SNR) of the PLL layer was calculated for each exposure time and echo time. For the images of Fig. 2, the SNRs of the low molecular weight PLL layer MVM beads were 23 ± 0.6, 20 ± 0.8 and 17 ± 0.1 for exposure times of 2, 6 and 20 min, respectively. These values correspond to a contrast enhancement relative to the minimal exposure time of 12% and 26% with the longer PLL exposures. This enhancement also is reflected in the calculated T_2* coefficients for the low molecular weight PLL layer of the MVM beads: 21.2, 20.2 and 16.6 ms for exposures of 2, 6 and 20 min, respectively. By comparison, the high molecular weight PLL layer of the MVM beads of Fig. 2 displayed only an average contrast enhancement relative to the minimum exposure of $2.3 \pm 1.0\%$ and T_2* coefficient of 18.1 ms. Meanwhile, the PLL enhancement seen in the MVG beads relative to the minimum exposure improved by $3.8 \pm 0.1\%$ and $8.6 \pm 0.02\%$ with increasing exposure times while the T_2* coefficient was calculated as 24.0, 23.3 and 22.7 ms for PLL exposures of 2, 6 and 30 min, respectively. Clearly, though not evident with the high molecular weight PLL, contrast enhancements could be identified and quantified for both alginates for the lower molecular weight PLL as a function of the exposure time.

In support of these images, the amount of PLL deposited on the alginate beads was quantified for the various experimental conditions examined in this study. Fig. 3 shows a bar graph depicting the amount of PLL deposited per milliliter of APA beads. These data show that when the lower molecular weight PLL was used, there was a statistically significant ($p < 0.05$) increase in the amount of PLL deposited on the alginate beads with increasing time of exposure. Furthermore, the quantities of PLL deposited on MVM based beads exposed for either 6 or 20 min to PLL were statistically higher ($p < 0.05$) than the corresponding MVG based beads. Conversely, when the higher molecular weight PLL was used, the amount of PLL deposited on the alginate beads could not be reliably quantified regardless of exposure time or alginate composition.

Fig. 4 shows a profile of the alginate/PLL thickness measured on four MVM APA beads (lower molecular weight PLL with 6 min exposure time) imaged with a GRE sequence and TE = 25 ms. Each point corresponds to a different slice through the bead, and thus, the values on the x-axis correspond to the relative location of the PLL measurement proceeding from one edge of a bead to the diametrically opposed side. The PLL thickness in each slice was measured by using a spatially defined histogram of MR signal intensity to count individual pixels in the MR microimage. Pixels were counted in the PLL thickness measurement if their signal intensity decreased by more

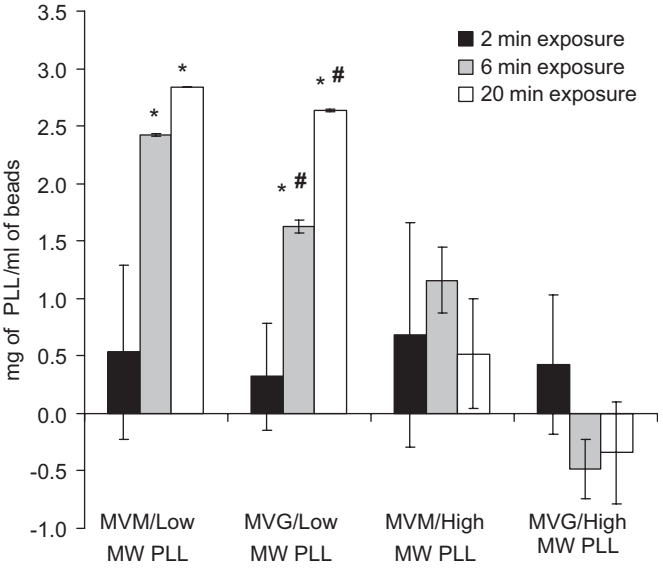

Fig. 3. A bar graph depicting the amount of PLL deposited per milliliter of alginate beads. Solid black, gray and white bars represent measurements based on 2, 6 and 20 min of exposure, respectively, between the various alginate and PLL combinations. Each bar is the average of duplicate measurements within the same experiment. This experiment was repeated three times with consistent results. An (*) indicates statistically significant differences ($P < 0.05$) between the 6 or 20 min exposures and to the corresponding alginate exposed for 2 min to PLL. A (#) indicates statistically significant differences ($P < 0.05$) between MVM and MVG alginates at the corresponding time exposures to PLL.

than 20% from the signal intensity of the center of the bead. In Fig. 4, the center point of the graph corresponds to the equator of the bead and represents the most accurate measurement of the PLL thickness at $40.6 \pm 6.2\,\mu m$. The increased apparent thickness at each edge of the profile is attributed to the curvature of the bead and the slice thickness of the images. Despite the detected changes in contrast intensity and PLL deposited on the beads, the thickness of the PLL layer measured by MR was constant for all combinations of PLL molecular weight, exposure time and alginate composition examined. In all cases, the thickness at the equator of the bead ranged between 35 and 50 μm. Furthermore, the thickness of the PLL layer did not change during the 30 days of culture, suggesting that the PLL layer is stable during this period.

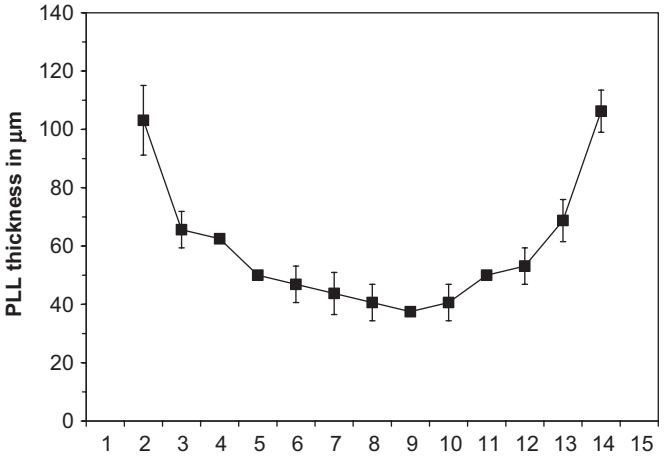

Fig. 4. A profile of PLL layer thickness measurements performed on MVM beads coated with the lower molecular weight PLL following a 6 min exposure. The beads were imaged with a GRE sequence and a TE = 25 ms. The *x*-axis represents arbitrary slice numbers with effective thickness of 50 μm. The error bars represent the standard deviation of the mean based on four measurements.

Using 3D volume rendering, the PLL layer was segmented to produce 3D images of the entire bead to assess the uniformity of the PLL coat, as seen in Fig. 5. The left panel shows a GRE image (a single slice from a 3D dataset acquired with TE = 25 ms) of a single APA bead (MVM alginate, lower molecular weight PLL, 6 min exposure). The panel on the right shows the 3D segmentation of the PLL shell generated from the GRE data set. The darker hue represents the PLL shell while the lighter hue represents the surrounding media. Segmentation was performed using AMIRA 3.1 (Mercury Computer Systems, Inc., Chelmsford MA). To simplify segmentation, a Gaussian filter was applied directly to the processed image dataset to enhance contrast between the internal bead and PLL layer and reduce the number of false positive points included in the rendered PLL layer. Segmentation was based on an automated selection of pixels determined by MR signal intensity thresholds (PLL layer fell between 15% and 30% of the peak signal intensity of the dataset), with nominal manual correction. The resulting image shows that there are no visible defects in the coating of the alginate beads with PLL, which underscores the continuity of this layer even at short exposure times.

3.2. Longitudinal changes in alginate NMR relaxation parameters due to long term culture

Fig. 6A illustrates the temporal changes in T_2 relaxation monitored over a month for MVG based alginate beads, while Fig. 6B shows the temporal changes for MVM based alginate beads. Our data show that MVG beads exhibit a decrease in T_2 relaxation time reaching a minimum value within 15 days. This decrease is markedly higher in

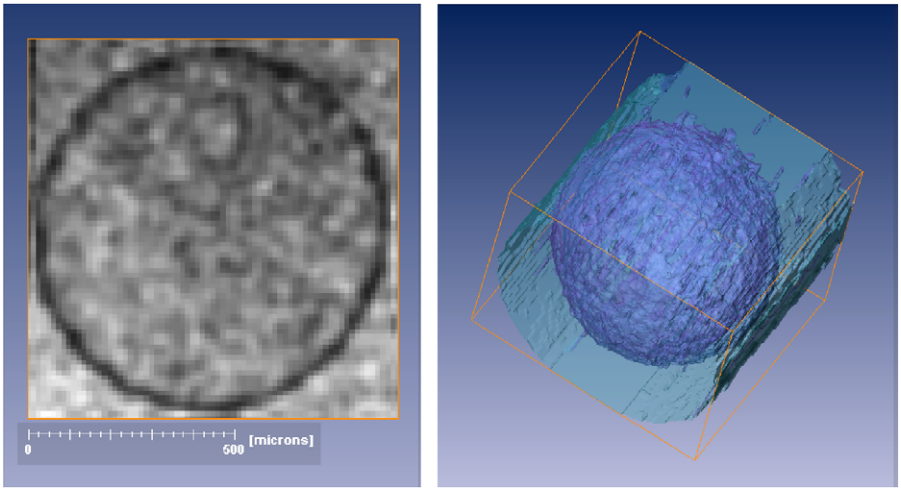

Fig. 5. The MR image on the left shows a single slice from a 3D GRE dataset with a TE = 25 ms of a single MVM alginate bead coated with the lower molecular weight PLL following a 6 min exposure. The dark contrast generated by the PLL layer has been segmented in the 3D rendering shown on the right. The darker hue of the 3D rendering represents the PLL shell while the lighter hue represents the surrounding media. Segmentation was performed based on pixel intensity values. Although a 3D Gaussian filter was applied to the image for the purpose of segmentation, the acquisition voxel size in the 3D data set was $12.5 \times 12.5 \times 12.5\,\mu m^3$.

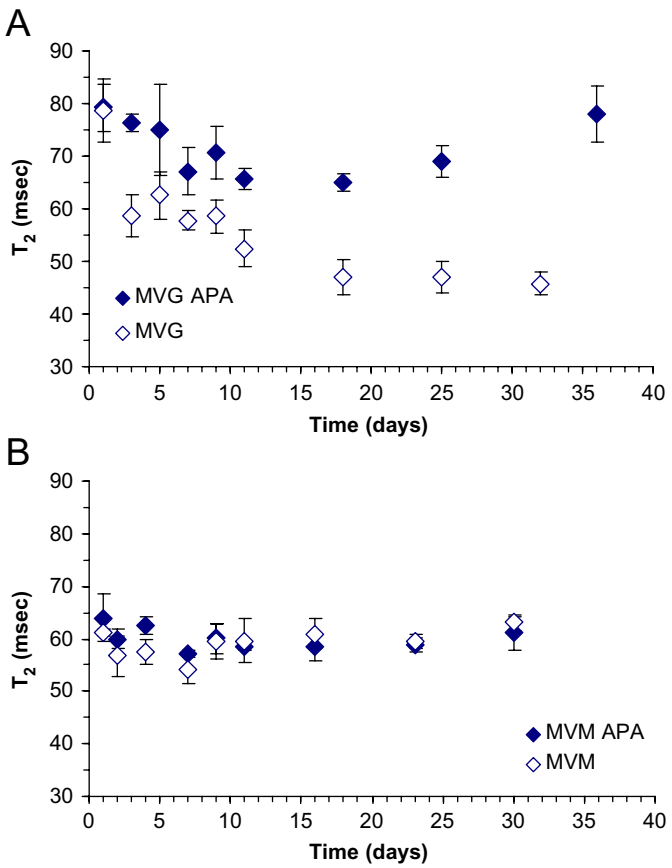

Fig. 6. (A) Temporal changes in the T_2 relaxation time of MVG alginate beads. Solid diamonds represent data acquired from MVG APA beads and open diamonds represent data acquired from MVG beads that were not coated with PLL. (B) Temporal changes in the T_2 relaxation time of MVM alginate beads. Solid diamonds represent data acquired from MVM APA beads and open diamonds represent data acquired from MVM beads that were not coated with PLL. The error bars represent the standard deviation of the T_2 relaxation measurement.

non-PLL coated beads. In contrast, MVM beads did not exhibit an appreciable change in T_2 relaxation for either PLL coated or non-coated beads. Diffusion-weighted images did not yield statistically significant temporal changes in ADC for any of the culture combinations examined (data not shown). This observation is in agreement with previous studies reporting a lack of change in ADC as a function of alginate composition [21,22].

4. Discussion

Visualization of the PLL layer in APA beads is not new; it was recently demonstrated with the use of fluorescent-labeled PLL and the aid of a confocal laser scanning microscope [30]. However, the MR techniques utilized in this study do not require the synthesis of fluorescent-labeled PLL. Commonly purchased PLL and standard SE and GRE MR sequences were utilized throughout this study. Our data show that T_2- and T_2*-weighted MR images are sensitive measures of the presence and thickness of the PLL layer. MR-based measurements of PLL thickness ranged from 35 to 50 μm for all combinations of PLL exposure times, PLL molecular weights and alginate compositions examined. This thickness is in agreement with data presented by Strand et al. (30–50 μm for exposure times up to 30 min), and it is attributed to the infiltration of PLL into the alginate matrix [30]. Such PLL infiltration is also reported in the studies by de Vos et al. [31] and Tam et al. [32]. This agreement between MR and non-MR methods further indicates that susceptibility effects do not significantly contribute to the thickness of the PLL layer in the MR images acquired under these conditions, which underscores the robust nature of the technique.

The contrast observed in either GRE or SE images is sensitive to changes in the interaction between lower molecular weight PLL and alginate beads regardless of their composition. Specifically, MVM or MVG beads displayed higher contrast (darker bead periphery) when exposed for 20 min than when exposed for 2 min. Similarly, the contrast of the PLL layer is higher (i.e. darker) in MVM beads than in corresponding MVG beads at a given exposure time. These observations were confirmed by the quantification of the PLL deposited on the beads. Thus, for the lower molecular weight PLL utilized in this study, the MR contrast of the PLL layer and the quantity of PLL deposited onto alginate beads correlated to the guluronic content of the beads and the exposure intervals.

Previous studies describing the interaction of similarly low molecular weight PLL and alginate are contradictory. The studies by Thu et al. [33,34] demonstrated that the binding affinity of PLL to alginate was lower for high guluronic content alginates, suggesting that more PLL can be deposited on alginates with a high mannuronic content. Conversely, the study by van Hoogmoed et al. demonstrated that alginate capsules made with a high guluronic content alginate contained 20% more PLL than similar capsules made with an intermediate guluronic content alginate [35]. The cause of this discrepancy is not fully understood. However, a new study by Tam et al. [32] suggests that the conformation of the alginate/PLL complex depends on the strength of the interaction between the two molecules. Specifically, when the interaction between alginate and PLL is weak (e.g., for high guluronic content alginates), the alginate/PLL complex has a random coil conformation. Alternatively, when the interaction between the two molecules is strong (e.g., for high mannuronic content alginates), the alginate/PLL complex has a specific helical conformation, namely an α–helix of interwoven with alginate [32]. Because the helical conformation is tighter than the random coil conformation, it will lead to more spin–spin interactions and shorten the T_2 relaxation time (i.e., darker contrast for the PLL/alginate interface). Therefore, it is possible that the difference in the contrast of the PLL layer in APA beads is attributed to the conformational differences of PLL/alginate complex and not solely to the quantity of PLL deposited on the beads.

In a similar vein, these data also demonstrate that the correlation between MR contrast and PLL exposure time on alginate does not hold for the higher molecular weight PLL utilized in the study. This is best illustrated by comparing preparations of MVG based beads. The contrast of the PLL layer on all MVG preparations is similar, regardless of the molecular weight of the PLL used to coat the beads. This observation suggests that similar quantities of PLL are deposited on these MVG beads. However, quantification of PLL showed statistically higher quantities of PLL were deposited on the beads when the lower molecular weight PLL was utilized. This is attributed to the restricted diffusion of the higher molecular weight PLL as it penetrates and interacts with alginate and it is in agreement with the study by Thu et al. [33]. Therefore, MR Microscopy provides an excellent method to assess non-invasively and non-destructively the interaction and dynamics of a polycation such as PLL with anionic hydrogels such as alginate.

A key concern with the use of alginate in tissue engineered constructs is the long-term stability of the alginate gel. Given that alginate gel is formed by the ionic interaction between negatively charged alginate molecules and positively charged calcium ions (or other similarly charged cations), it is reasonable to hypothesize that calcium ions may diffuse out of the alginate matrix during a prolonged culture. This process may cause the alginate/calcium bond to weaken, resulting in a weaker gel that may dissolve or break. A recent study by Simpson et al. [36] demonstrated that alginates with a higher guluronic content are more susceptible to changes in Ca^{+2} ion concentration. Thus, it is reasonable to assume that the "egg-box" configuration [37] of the gelled MVG alginate will weaken with time in culture, due to the diffusion of Ca^{+2} ions, causing a collapse of the gel structure and a decrease in gel porosity. From the NMR perspective, this decrease should manifest as a decrease in T_2 values, which is indicated by the data presented in Fig. 6. The fact that the observed decrease in T_2 is more pronounced in non-PLL-coated MVG beads than in PLL coated beads supports a previous study suggesting that the PLL layer hinders the transport of Ca^{+2} ions across the PLL layer [22]. Thus, the MVG gel microstructure is better maintained in PLL-coated beads than in non-coated beads.

Metabolic studies with βTC3 cells encapsulated in MVG APA beads show that encapsulated cells begin to grow after 20 days in culture, whereas βTC3 cells encapsulated in MVM grow continuously from the onset of the culture [38]. T_2 data presented in Fig. 6, show that MVG beads undergo a gel microstructure re-organization during the first 2 weeks of culture. It is particularly interesting to note that the minimum T_2 values measured from MVG APA beads are similar to those measured from MVM beads throughout the study. These observations suggest that MVG gels re-organize during *in vitro* culture, reaching a configuration that is more conducive to cell growth. One way to prevent the re-organization of the MVG gel is to periodically wash the alginate beads in $CaCl_2$ as was recently demonstrated [36]. Unlike MVG alginate, MVM alginate does not experience the same change in porosity due to the weaker Ca^{+2}/alginate interaction. Consequently, the MVM microstructure does not undergo a significant re-organization over the culture period, which is consistent with the static T_2 value measured in this study.

Finally, T_2 values for MVG and MVM alginate beads measured 24 h after encapsulation and maintained in DMEM media were compared to measurements reported previously with similar beads maintained in $CaCl_2$ for a day [22]. While T_2 values of MVG beads were similar in both media conditions, T_2 values for MVM beads maintained in DMEM were higher than those reported for beads maintained in $CaCl_2$. This observation suggests that MVG alginate beads maintained their initial organization after 24 h of DMEM incubation while MVM alginate beads underwent a rapid alteration during this period. This difference may be attributed to the different swelling properties between MVG and MVM alginates. High guluronic content alginates maintain their rigid structure initially due to their strong Ca^{2+}/alginate interaction, while high mannuronic content alginates swell more readily resulting in an increase in T_2 once the presence of external $CaCl_2$ is removed. Notably, the swelling of the MVM alginate takes place rapidly during this first 24-h timeframe, after which the structure of the MVM bead remains constant for the remainder of the culture time as reflected by the T_2 measurements over the 30-day period.

5. Conclusion

In summary, we have demonstrated that MR microscopy can non-invasively and non-destructively visualize and quantify the PLL layer and monitor temporal changes in the structure of alginate beads during a prolonged culture. The data show that the thickness of the PLL layer at the periphery of alginate beads is between 35 and 50 μm regardless of the alginate composition or the time of exposure to the PLL solution (up to 20 min). The data also show that high guluronic content alginate beads undergo reorganization of their gel structure during an *in vitro* culture, while high mannuronic content alginate beads are not susceptible to such changes under similar culture conditions. It should be emphasized that the imaging techniques utilized in this study are generic and can be applied to study other hydrogels and/or other polycation layers.

Acknowledgments

The authors would like to acknowledge the financial support of the NIH through Grants R01 DK56890, R01 DK47858, and P41 RR16105. All MR data were obtained at the Advanced Magnetic Resonance Imaging and Spectroscopy (AMRIS) facility in the McKnight Brain Institute of the University of Florida. Pilot funds for

imaging time were provided by AMRIS and the National High Magnetic Field Laboratory.

References

[1] Constantinidis I, Sambanis A. Non-invasive monitoring of tissue engineered constructs by nuclear magnetic resonance methodologies. Tissue Eng 1998;4:9–17.

[2] Burg KJ, Delnomdedieu M, Beiler RJ, Culberson CR, Greene KG, Halberstadt CR, et al. Application of magnetic resonance microscopy to tissue engineering: a polylactide model. J Biomed Mater Res 2002;5:380–90.

[3] Neves AA, Medcalf N, Brindle K. Functional assessment of tissue-engineered meniscal cartilage by magnetic resonance imaging and spectroscopy. Tissue Eng 2003;9:51–62.

[4] Papas KK, Long Jr. RC, Constantinidis I, Sambanis A. Role of ATP and P_i on the mechanism of insulin secretion in the mouse insulinoma βTC3 cell line. Biochem J 1997;326:807–14.

[5] Papas KK, Long Jr. RC, Constantinidis I, Sambanis A. Development of a bioartificial pancreas: I. Long-term propagation and basal and induced secretion from entrapped βTC3 cell cultures. Biotechnol Bioeng 1999;66:219–30.

[6] Papas KK, Long Jr. RC, Constantinidis I, Sambanis A. Development of a bioartificial pancreas: II. Effects of oxygen on long-term entrapped βTC3 cell cultures. Biotechnol Bioeng 1999;66:231–7.

[7] Papas KK, Long Jr. RC, Sambanis A, Constantinidis I. Effects of short-term hypoxia on a bioartificial pancreatic construct. Cell Transp 2000;9:415–22.

[8] Long Jr. RC, Papas KK, Sambanis A, Constantinidis I. *In vitro* monitoring of total choline levels in a bioartificial pancreas: ^{1}H NMR spectroscopic studies of the effects of oxygen level. J Magn Reson 2000;146:49–57.

[9] Stabler CL, Long Jr. RC, Constantinidis I, Sambanis A. Noninvasive measurement of viable cell number in tissue engineered constructs *in vitro* using ^{1}H NMR spectroscopy. Tissue Eng 2005;11:404–14.

[10] Stabler CL, Long Jr. RC, Constantinidis I, Sambanis A. *In vivo* noninvasive monitoring of viable cell number in tissue engineered constructs using ^{1}H NMR spectroscopy. Cell Transp 2005;14:139–49.

[11] Soon-Shiong P, Feldman E, Nelson R, Heintz T, Yao Q, Yao Z, et al. Long-term reversal of diabetes by the injection of immunoprotected islets. Proc Natl Acad Sci USA 1993;90:5843–7.

[12] Reach G. Bioartificial pancreas. Diabetic Med 1993;10:105–9.

[13] Lim F, Sun AM. Microencapsulated islets as bioartificial endocrine pancreas. Science 1980;210:908–10.

[14] Lanza RP, Chick WL. Transplantation of encapsulated cells and tissues. Surgery 1997;121:1–9.

[15] Sambanis A, Papas KK, Flanders PC, Long Jr. RC, Kang H, Constantinidis I. Towards the development of a bioartificial pancreas: immunoisolation and NMR monitoring of mouse insulinomas. Cytotechnology 1994;15:351–63.

[16] Constantinidis I, Sambanis A. Towards the development of artificial endocrine tissues: ^{31}P NMR spectroscopic studies of immunoisolated, insulin-secreting AtT-20 cells. Biotechnol Bioeng 1995;47:431–43.

[17] Hicks BA, Stein R, Efrat S, Grant S, Hanahan D, Demetriou AA. Transplantation of β cells from transgenic mice into nude athymic diabetic rats restores glucose regulation. Diabete Res Clin Pract 1991;14:157–64.

[18] Benson JP, Papas KK, Constantinidis I, Sambanis A. Towards the development of a bioartificial pancreas: effects of poly-L-lysine on alginate beads with βTC3 cells. Cell Transp 1997;6:395–402.

[19] Lanza RP, Chick WL. Immunoisolation: at a turning point. Immunol Today 1997;18:135–9.

[20] Duez JM, Mestdagh M, Demeure R, Goudemant JF, Hills BP, Godward J. NMR studies of calcium-induced alginate gelation. Part I—MRI tests of gelation models. Magn Reson Chem 2000;38:324–30.

[21] Hills BP, Godward J, Debatty M, Barras L, Saturio CP, Ouwerx C. NMR studies of calcium induced alginate gelation. Part II. The internal bead structure. Magn Reson Chem 2000;38:719–28.

[22] Simpson NE, Grant SC, Blackband SJ, Constantinidis I. NMR properties of alginate microbeads. Biomaterials 2003;24:4941–8.

[23] Emmerichs N, Wingender J, Flemming H-C, Mayer C. Interaction between alginates and manganese cations: identification of preferred cation binding sites. Int J Biol Macromol 2004;34:73–9.

[24] Manz B, Hillgartner M, Zimmermann H, Zimmermann D, Volke F, Zimmermann U. Cross-linking properties of alginate gels determined by using advanced NMR imaging and $Cu^{(2+)}$ as contrast agent. Eur Biophys J 2004;33:50–8.

[25] Thu B, Gaserod O, Paus D, Mikkelsen A, Skjak-Braek G, Toffanin R, et al. Inhomogeneous alginate gel spheres: an assessment of the polymer gradients by synchrotron radiation-induced X-ray emission, magnetic resonance microimaging, and mathematical modeling. Biopolymers 2000;53:60–71.

[26] As HV, Lens P. Use of ^{1}H NMR to study transport processes in porous biosystems. J Ind Microbiol Biotechnol 2001;26:43–52.

[27] Skjak-Braek G, Grasdale H, Smidsrod O. Inhomogeneous polysaccharide ionic gels. Carbohyd Polym 1989;10:31–54.

[28] Webb AG, Grant SC. Signal-to-noise and magnetic susceptibility trade-offs in solenoidal microcoils for NMR. J Magn Reson B 1996;113:83–7.

[29] Hsu EW, Schoeniger JS, Bowtell R, Aiken NR, Horsman A, Blackband SJ. A modified imaging sequence for accurate T2 measurements using NMR microscopy. J Magn Reson B 1995;109:66–9.

[30] Strand BL, Yrr AM, Espevik T, Skjak-Braek G. Visualization of alginate-poly-L-lysine-alginate microcapsules by confocal lazer scanning microscopy. Biotechnol Bioeng 2003;82:386–94.

[31] de Vos P, van Hoogmoed CG, Busscher HJ. Chemistry and biocompatibility of alginate-PLL capsules for immunoprotection of mammalian cells. J Biomed Mater Res 2002;60:252–9.

[32] Tam SK, Dusseault J, Polizu S, Menard M, Halle JP, Yahia L. Physicochemical model of alginate-poly-L-lysine microcapsules defined at the micrometric/nanometric scale using ATR-FTIR, XPS, and ToF-SIMS. Biomaterials 2005;26:6950–61.

[33] Thu B, Bruheim P, Espevik T, Smidsrod O, Soon-Shiong P, Skjak-Braek G. Alginate polycation microcapsules. I. Interaction between alginate and polycation. Biomaterials 1996;17:1031–40.

[34] Thu B, Bruheim P, Espevik T, Smidsrod O, Soon-Shiong P, Skjak-Braek G. Alginate polycation microcapsules. II. Some functional properties. Biomaterials 1996;17:1069–79.

[35] van Hoogmoed CG, Busscher HJ, de Vos P. Fourier transform infrared spectroscopy studies of alginate-PLL capsules with varying compositions. J Biomed Mater Res 2003;67A:172–8.

[36] Simpson NE, Stabler CL, Sambanis A, Constantinidis I. The role of the $CaCl_2$-guluronic acid interaction on alginate encapsulated βTC3 cells. Biomaterials 2004;25:2603–10.

[37] Grant GT, Morris ER, Rees DA, Smith PJC, Thom D. Biological interactions between polysaccharides and divalent cations: the egg-box model. FEBS Lett 1973;32:195–8.

[38] Stabler C, Wilks K, Sambanis A, Constantinidis I. The effects of alginate composition on encapsulated βTC3 cells. Biomaterials 2001;22:1301–10.